LETTERS

Broad-band optical parametric gain on a silicon photonic chip

Mark A. Foster[1], Amy C. Turner[2], Jay E. Sharping[1], Bradley S. Schmidt[2], Michal Lipson[2] & Alexander L. Gaeta[1]

Developing an optical amplifier on silicon is essential for the success of silicon-on-insulator (SOI) photonic integrated circuits. Recently, optical gain with a 1-nm bandwidth was demonstrated using the Raman effect[1–9], which led to the demonstration of a Raman oscillator[10,11], lossless optical modulation[12] and optically tunable slow light[13]. A key strength of optical communications is the parallelism of information transfer and processing onto multiple wavelength channels. However, the relatively narrow Raman gain bandwidth only allows for amplification or generation of a single wavelength channel. If broad gain bandwidths were to be demonstrated on silicon, then an array of wavelength channels could be generated and processed, representing a critical advance for densely integrated photonic circuits. Here we demonstrate net on/off gain over a wavelength range of 28 nm through the optical process of phase-matched four-wave mixing in suitably designed SOI channel waveguides. We also demonstrate wavelength conversion in the range 1,511–1,591 nm with peak conversion efficiencies of +5.2 dB, which represents more than 20 times improvement on previous four-wave-mixing efficiencies in SOI waveguides[14–17]. These advances allow for the implementation of dense wavelength division multiplexing in an all-silicon photonic integrated circuit. Additionally, all-optical delays[18], all-optical switches[19], optical signal regenerators[20] and optical sources for quantum information technology[21], all demonstrated using four-wave mixing in silica fibres, can now be transferred to the SOI platform.

Amplification through four-wave mixing (FWM)[22] is a nonlinear optical process derived from the third-order nonlinear susceptibility, $\chi^{(3)}$, of a material. In silicon, the lowest-order optical nonlinearity is third order, which gives rise to an intensity dependent refractive index $n = n_0 + n_2 I$, where n_0 is the linear refractive index, $n_2 = 12\pi^2\chi^{(3)}/n_0 c$ is the nonlinear index coefficient, c is the speed of light, and I is the optical intensity. The measured n_2 values in silicon are in the range $(4–9) \times 10^{-14}$ cm^2 W^{-1} (refs 14, 23, 24), which is approximately 200 times that of silica glass. As shown in Fig. 1, in FWM two pump photons at frequency ω_{pump} are converted to signal and idler photons at respective frequencies ω_{signal} and ω_{idler} such that $2\omega_{pump} = \omega_{signal} + \omega_{idler}$, which can lead to amplification of the signal wave. In addition, the pump wave experiences self-phase modulation (SPM) and induces cross-phase modulation (XPM) on the signal and idler waves, which is twice as large as the pump SPM. The gain experienced by the signal wave depends on the phase-mismatch Δk between the propagation constants of the waves and on the nonlinear effects of SPM and XPM such that[22]

$$\Delta k = 2\gamma P_{pump} - \Delta k_L \quad (1)$$

where $\Delta k_L = 2k_{pump} - k_{signal} - k_{idler}$ is the phase mismatch due to linear dispersion, k_{pump}, k_{signal} and k_{idler} are respectively the pump, signal and idler wavenumbers, P_{pump} is the pump power, $\gamma = \omega_{pump} n_2/cA_{eff}$ is the effective nonlinearity of the waveguide, and A_{eff} is the effective area of the propagating mode. The FWM gain coefficient g is given by[22]

$$g = \left[\gamma P_{pump}\Delta k_L - (\Delta k_L/2)^2\right]^{\frac{1}{2}} \quad (2)$$

and neglecting the effects of pump depletion, the observed signal gain G_{signal} due to FWM is[22]

$$G_{signal} = \frac{P^{out}_{signal}}{P^{in}_{signal}} = 1 + \left(\frac{\gamma P_{pump}}{g}\sinh(gL)\right)^2 \quad (3)$$

where P^{out}_{signal} and P^{in}_{signal} are the output and input signal powers, respectively, and L is the interaction length. The peak gain occurs when the phase shift due to SPM and XPM is compensated by the mismatch in the propagation constants of the pump, signal and idler waves. This requires the pump wave to have a larger propagation vector than the average of the signal and idler, which occurs when the group-velocity dispersion (GVD) is anomalous (that is, $d^2k_{pump}/d\omega^2 < 0$). In optical fibres, FWM is routinely implemented in the telecommunications band beyond 1.3 μm, where the GVD of silica glass is anomalous[22].

Four-wave mixing was previously observed in SOI waveguides with normal GVD, but the conversion occurred over a narrow band, the efficiencies were minimal, and net gain was not observed owing to the lack of phase-matching[14–17]. At wavelengths near 1.5 μm, silicon exhibits very large normal GVD owing to the proximity of the absorption band edge at 1.1 μm. Waveguide confinement introduces anomalous GVD, which is used in silica glass fibres to create net anomalous-GVD regions[25] several octaves from any material resonance. However, it is not clear that this waveguide contribution in highly confining SOI waveguides can overcome the material dispersion so close to the absorption band and yield net anomalous

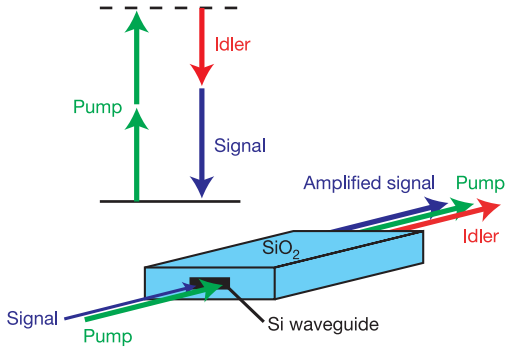

Figure 1 | Four-wave mixing with a degenerate pump. The four-wave-mixing process involves the conversion of two pump photons to a signal photon and an idler photon (top). By suitable design of the waveguide, momentum conservation (that is, phase-matching) is also satisfied and amplification of the signal occurs (bottom).

[1]School of Applied and Engineering Physics, [2]School of Electrical and Computer Engineering, Cornell University, Ithaca, New York 14853, USA.

GVD. We investigate this issue through simulations using a custom full-vector finite difference mode solver to calculate the GVD of the propagating mode. For accurate results, it is important to include the coupled effects of material and waveguide dispersion rather than treating them independently. For a small range of waveguide shapes and sizes, we predict[26,27] and observe[27] the anomalous GVD required for phase-matching. In Fig. 2a, we plot the GVD for waveguides with different cross-sections, and the predicted FWM gain for a 2-cm propagation length and a 1-W peak pump power is shown in Fig. 2b. The waveguide with anomalous GVD (300 nm × 600 nm) allows for phase-matching and is predicted to have a broad region of large amplification. In comparison, the smallest (200 nm × 400 nm) and largest (1.0 μm × 1.5 μm) waveguides have normal GVD and show minimal gain. The use of birefringence was suggested to achieve phase-matching in larger waveguides[28], but this additional complexity is not required for waveguides that exhibit anomalous GVD.

We experimentally investigate FWM in SOI waveguides with various cross-sectional geometries fabricated as previously described[29] but with a 1-μm buried oxide layer. The pump and signal pulses are each derived from a femtosecond optical parametric oscillator centred at 1,550 nm with a 75-MHz repetition rate. The pump pulses are filtered to a 1-nm bandwidth centred at 1,550 nm, and the signal pulses are filtered to a 1.5-nm bandwidth, tunable from 1,510 nm to 1,590 nm. After filtering, the temporal durations of the pump and signal pulses are 3.5 ps and 2.4 ps, respectively. The pump pulses are amplified in an erbium-doped fibre amplifier and combined with the signal pulses using a wavelength division multiplexer. Both the pump and signal arms incorporate fibre polarization controllers to achieve TE polarization in the silicon waveguide. The light is coupled into the waveguide using a tapered lens fibre and an inverse taper mode converter on the silicon chip[29], which results in a

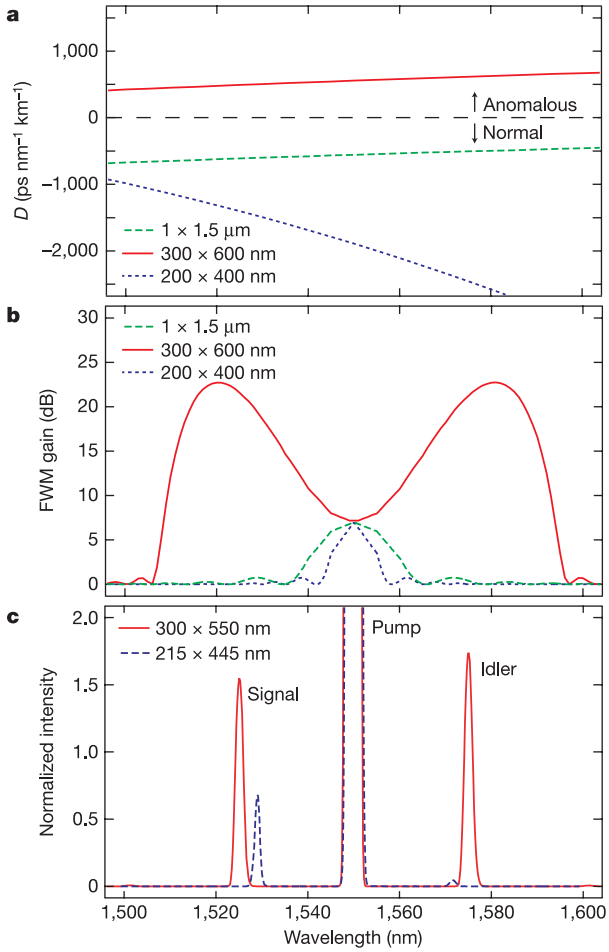

Figure 2 | Anomalous group-velocity dispersion and phase-matched four-wave mixing. **a**, Simulated group-velocity dispersion (GVD), denoted *D*, and **b**, four-wave mixing (FWM) gain for silicon waveguides with several cross-sectional dimensions. The FWM gain is calculated assuming a 1-W peak pump power and a 2-cm-long waveguide. The 300 nm × 600 nm waveguide exhibits anomalous GVD ($D > 0$), allowing for phase-matching and large amplification. The smallest waveguide (200 nm × 400 nm) and largest waveguide (1 μm × 1.5 μm) have normal GVD ($D < 0$) and thus minimal gain. **c**, Experimentally observed FWM spectra from waveguides exhibiting anomalous GVD (300 nm × 550 nm) and near-zero GVD (215 nm × 445 nm). Both plots are normalized to the signal power with the pump off.

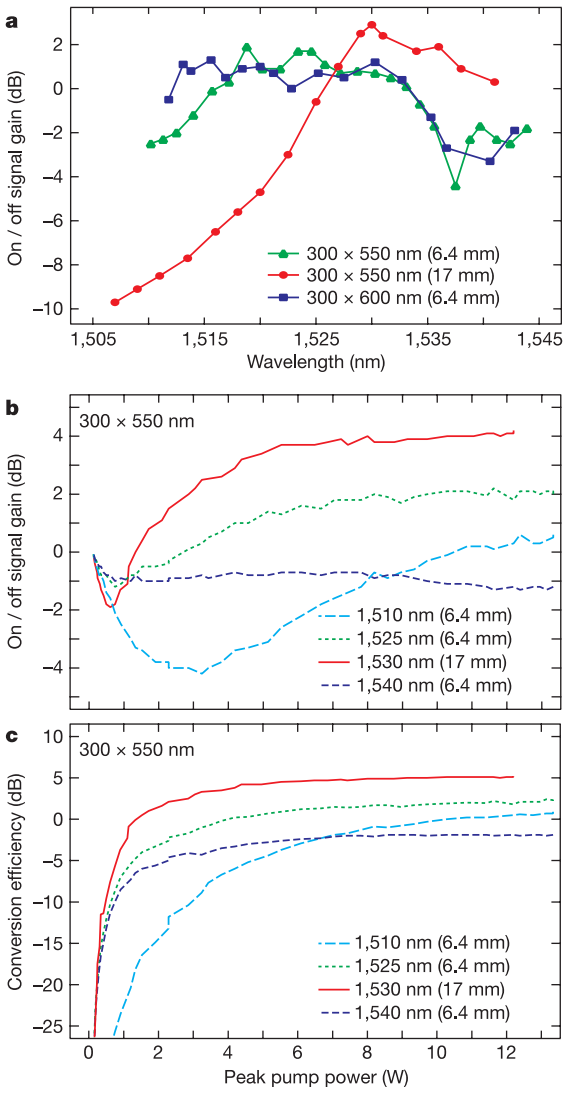

Figure 3 | Experimentally measured amplification. **a**, Measured on/off signal gain as a function of signal wavelength for several waveguide cross-sectional areas and lengths, which illustrates the gain sensitivity to waveguide dimensions. The key in **a** shows 'waveguide dimensions (length)', whereas the key in **b** and **c** shows 'signal wavelength (waveguide length)'. We observe a larger shift in the peak of the gain from the pump wavelength as the waveguide width is increased, which results from the reduced magnitude of anomalous GVD. **b**, **c**, Measured on/off signal gain (**b**) and idler conversion efficiency (**c**) as functions of peak pump power inside the waveguide for 6.4-mm- and 17-mm-long waveguides with 300 nm × 550 nm cross-sections. Once a sufficient pump power is reached to achieve phase-matching at the observed wavelength, we measure a net nonlinear amplification of the signal.

measured coupling loss ranging from −12.3 dB to −13.3 dB. The large loss was due to poor overlap between the mode of the lens fibre and that of the inverse taper. The measured linear propagation loss in the waveguides ranges from $-1.1\,\mathrm{dB\,cm^{-1}}$ to $-1.4\,\mathrm{dB\,cm^{-1}}$ at 1,550 nm. These values are determined by comparing the loss in waveguides of two lengths differing by 7.4 mm. These results were compared over six different waveguides for a consistent measurement. All the waveguides incorporated the same number of bends and taper couplers. The inverse taper ensures excitation of the fundamental mode for multi-mode waveguides. The light leaving the silicon waveguide is collected and sent to an optical spectrum analyser for detection.

Typically observed FWM signals for waveguides with anomalous GVD and near-zero GVD are shown in Fig. 2c. Using a 6.4-mm-long 300 nm × 550 nm waveguide with a peak pump power of 11.0 W inside the waveguide, we observe net gain on the signal (1.9 dB) and highly efficient wavelength conversion (+2.4 dB). We expect that the idler wave carries more power than the signal owing to temporal and wavelength dependent effects of the nonlinear losses. For comparison, we plot the signal with near-zero GVD in an 8-mm-long, 215 nm × 445 nm waveguide with a peak pump power of 8.0 W inside the waveguide. Despite the higher nonlinearity of this waveguide, FWM yields a net loss on the signal (−1.7 dB) and small conversion efficiency (−13.2 dB) owing to the absence of phase-matching.

The gain bandwidth for this system is illustrated in Fig. 3a, which shows the measured on/off signal gain as a function of signal wavelength for several waveguide cross-sections and lengths. We define the on/off signal gain and idler conversion efficiency as the signal and idler power, respectively, leaving the waveguide with the pump beam on divided by the signal power leaving the waveguide with the pump beam off[16,17]. The effects of phase-matching are evident as the peak of the gain is shifted significantly from the pump wavelength. As expected, the magnitude of the shift increases for waveguides with decreasing GVD. Experimentally, we observe smaller gain than predicted by the simple model used for Fig. 2b owing to the combined effects of nonlinear absorption, free-carrier absorption and pump depletion. In Fig. 3b and c we plot the measured on/off signal gain (Fig. 3b) and idler conversion efficiency (Fig. 3c) as functions of peak pump power inside the waveguide for a 300 nm × 550 nm, 6.4-mm-long waveguide and several signal wavelengths. From these curves, it is evident that the nonlinear loss mechanisms of two-photon absorption[23,24] and free-carrier generation[4,30] are dominant at low pump powers. With increased pump power, the FWM process becomes phase-matched at the wavelength of observation, and for wavelengths sufficiently far from the pump, this gain eventually exceeds the nonlinear losses, resulting in net nonlinear gain. For the 6.4-mm-long waveguides, we observe a peak net on/off gain of 1.9 dB, and a net on/off gain can be produced from 1,512 nm to 1,535 nm with a pump laser tuned to 1,550 nm (Fig. 3a).

A consequence of this FWM process is the ability to perform efficient wavelength conversion. As seen in Fig. 3c, we observe peak conversion efficiencies ranging from +3 dB to −2 dB for signal wavelengths from 1,511 nm to 1,545 nm, which corresponds to idler wavelengths from 1,555 nm to 1,591 nm. We were limited to this range owing to the bandwidth of the femtosecond source pulses. Larger wavelength conversion bandwidths are expected, as we observe conversion efficiency of +3 dB at the edge (1,511 nm) of the signal tuning range.

To offset nonlinear absorption and increase the gain, we implement a longer waveguide of 17-mm length. This waveguide has a cross-section of 300 nm × 550 nm and four 100-μm-radius bends. The on/off signal gain is plotted as a function of wavelength in Fig. 3a. For a peak pump power of 4.2 W inside the waveguide, we see a peak on/off gain of 2.9 dB and an on/off gain bandwidth from 1,525 nm to 1,540 nm. Nonlinear absorption dominates outside the phase-matching region and reaches −9.7 dB. In Fig. 3b and c, we plot the on/off signal gain and idler conversion efficiency as functions of pump power for this longer waveguide, and we observe a peak gain and efficiency of 4.2 dB and +5.2 dB, respectively. We expect that optimization of the waveguide length and GVD will yield further reductions in pump power requirements. Including linear propagation loss ($-1.4\,\mathrm{dB\,cm^{-1}}$), this 4.2 dB on/off gain yields a net gain of 1.8 dB on the signal after 1.7 cm of propagation. Observation of net gain allows for the possibility of parametric oscillation with the inclusion of on-chip resonating structures for feedback. Furthermore, comparing the largest observed gain to the observed loss outside the FWM bandwidth, we calculate the gain arising from FWM to be at least 13.9 dB.

We have demonstrated broadband phase-matched FWM optical amplification and frequency conversion in an all-silicon photonic chip. We expect that additional increases in performance can be achieved by implementing techniques to remove free carriers and minimize nonlinear losses[9,11]. The ability to amplify and convert wavelengths over this wide range with a single pump laser, all within the communications band, dramatically enhances the signal processing capabilities of all-silicon photonic integrated circuits. Following these findings, we expect that numerous applications of FWM, already demonstrated in silica optical fibers, will be transferred to silicon photonic integrated circuits, including all-optical switching, optical signal regeneration and optical sources for quantum information technology.

Received 9 January; accepted 23 May 2006.

1. Claps, R., Dimitropoulos, D., Raghunathan, V., Han, Y. & Jalali, B. Observation of stimulated Raman amplification in silicon waveguides. *Opt. Express* **11,** 1731–1739 (2003).
2. Espinola, R. L., Dadap, J. I., Osgood, R. M. Jr, McNab, S. J. & Vlasov, Y. A. Raman amplification in ultrasmall silicon-on-insulator wire waveguides. *Opt. Express* **12,** 3713–3718 (2004).
3. Liu, A., Rong, H., Paniccia, M., Cohen, O. & Hak, D. Net optical gain in a low loss silicon-on-insulator waveguide by stimulated Raman scattering. *Opt. Express* **12,** 4261–4268 (2004).
4. Rong, H. *et al.* Raman gain and nonlinear optical absorption measurements in a low-loss silicon waveguide. *Appl. Phys. Lett.* **85,** 2196–2198 (2004).
5. Xu, Q., Almeida, V. R. & Lipson, M. Time-resolved study of Raman gain in highly confined silicon-on-insulator waveguides. *Opt. Express* **12,** 4437–4442 (2004).
6. Liang, T. K. & Tsang, H. K. Efficient Raman amplification in silicon-on-insulator waveguides. *Appl. Phys. Lett.* **85,** 3343–3345 (2004).
7. Boyraz, O. & Jalali, B. Demonstration of 11 dB fiber-to-fiber gain in a silicon Raman amplifier. *Electron. Express* **1,** 429–434 (2004).
8. Xu, Q., Almeida, V. R. & Lipson, M. Demonstration of high Raman gain in a submicrometer-size silicon-on-insulator waveguide. *Opt. Lett.* **30,** 35–37 (2005).
9. Jones, R. *et al.* Net continuous wave optical gain in a low loss silicon-on-insulator waveguide by stimulated Raman scattering. *Opt. Express* **13,** 519–525 (2005).
10. Rong, H. *et al.* An all-silicon Raman laser. *Nature* **433,** 292–294 (2005).
11. Rong, H. *et al.* A continuous-wave Raman silicon laser. *Nature* **433,** 725–728 (2005).
12. Jones, R. *et al.* Lossless optical modulation in a silicon waveguide using stimulated Raman scattering. *Opt. Express* **13,** 1716–1723 (2005).
13. Okawachi, Y. *et al.* All-optical slow-light on a photonic chip. *Opt. Express* **14,** 2317–2322 (2006).
14. Fukuda, H. *et al.* Four-wave mixing in silicon wire waveguides. *Opt. Express* **13,** 4629–4637 (2005).
15. Espinola, R. L., Dadap, J. I., Osgood, R. M. Jr, McNab, S. J. & Vlasov, Y. A. C-band wavelength conversion in silicon photonic wire waveguides. *Opt. Express* **13,** 4341–4349 (2005).
16. Yamada, K. *et al.* All-optical efficient wavelength conversion using silicon photonic wire waveguide. *IEEE Photon. Technol. Lett.* **18,** 1046–1048 (2006).
17. Rong, H., Kuo, Y. H., Liu, A., Paniccia, M. & Cohen, O. High efficiency wavelength conversion of 10 Gb/s data in silicon waveguides. *Opt. Express* **14,** 1182–1188 (2006).
18. Sharping, J. E. *et al.* All-optical, wavelength and bandwidth preserving, pulse delay based on parametric wavelength conversion and dispersion. *Opt. Express* **13,** 7872–7877 (2005).
19. Lin, Q. *et al.* 40-Gb/s optical switching and wavelength multicasting in a two-pump parametric device. *IEEE Photon. Technol. Lett.* **17,** 2376–2378 (2005).
20. Ciaramella, E. & Trillo, S. All-optical reshaping via four-wave mixing in optical fibers. *IEEE Photon. Technol. Lett.* **12,** 849–851 (2000).

21. Li, X., Voss, P. L., Sharping, J. E. & Kumar, P. Optical-fiber source of polarization-entangled photons in the 1550 nm telecom band. *Phys. Rev. Lett.* **94,** 053601 (2005).
22. Hansryd, J., Andrekson, A., Westlund, M., Li, J. & Hedekvist, P. Fiber-based optical parametric amplifiers and their applications. *IEEE Select. Topics Quant. Electron.* **8,** 506–520 (2002).
23. Tsang, H. K. *et al.* Optical dispersion, two-photon absorption and self-phase modulation in silicon waveguides at 1.5 μm wavelength. *Appl. Phys. Lett.* **80,** 416–418 (2002).
24. Dinu, M., Quochi, F. & Garcia, H. Third-order nonlinearities in silicon at telecom wavelengths. *Appl. Phys. Lett.* **82,** 2954–2956 (2003).
25. Foster, M. A., Moll, K. D. & Gaeta, A. L. Optimal waveguide dimensions for nonlinear interactions. *Opt. Express* **12,** 2880–2887 (2004).
26. Raghunathan, V., Claps, R., Dimitropoulos, D. & Jalali, B. Parametric Raman wavelength conversion in scaled silicon waveguides. *J. Lightwave Technol.* **23,** 2094–2102 (2005).
27. Turner, A. C. *et al.* Tailored anomalous-group velocity dispersion in silicon channel waveguides. *Opt. Express* **14,** 4357–4362 (2006).
28. Dimitropoulos, D., Raghunathan, V., Claps, R. & Jalali, B. Phase-matching and nonlinear optical processes in silicon waveguides. *Opt. Express* **12,** 149–160 (2004).
29. Almeida, V. R., Panepucci, R. R. & Lipson, M. Nanotapers for compact mode conversion. *Opt. Lett.* **28,** 1302–1304 (2003).
30. Liang, T. K. & Tsang, H. K. Role of free carriers from two-photon absorption in Raman amplification in silicon-on-insulator waveguides. *Appl. Phys. Lett.* **84,** 2745–2747 (2004).

Acknowledgements We acknowledge discussions with Y. Okawachi. This work was supported by the Center for Nanoscale Systems, supported by the NSF and the New York State Office of Science, Technology & Academic Research. M.A.F., J.E.S. and A.L.G. acknowledge support from the DARPA DSO Slow-Light Program.

Author Information Reprints and permissions information is available at npg.nature.com/reprintsandpermissions. The authors declare no competing financial interests. Correspondence and requests for materials should be addressed to A.L.G. (a.gaeta@cornell.edu).